Langmuir
Article
pubs.acs.org/Langmuir

Prediction of Coating Thickness in the Convective Assembly Process

Yoon Dong Jung and Kyung Hyun Ahn*

School of Chemical and Biological Engineering, Institute of Chemical Process, Seoul National University, Seoul, 151-744, Korea

ABSTRACT: Convective assembly is a coating method to fabricate thin films with ordered particle structures that can be used extensively for biochemical sensors, data storage devices, optical devices, and other applications. The fluid flow into or through the close-packed region causes the convective assembly, and it is important to understand the formation mechanism of the close-packed region. In this paper, the length of the close-packed region was predicted, and the dimensionless coating thickness as well as the dimensionless length of the close-packed region was found to be the functions of only three dimensionless variables: two capillary numbers and the initial volume fraction. From the modeling results, coating process regime maps that predict the dimensionless coating thickness in terms of the dimensionless variables were created. In addition, the length of the close-packed region was measured under various coating conditions to validate the model prediction. The experiments firmly supported the model predictions.

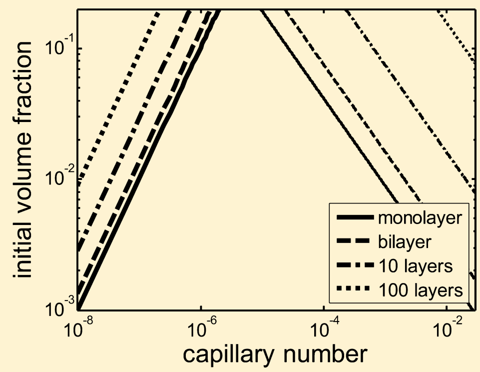

1. INTRODUCTION

Particulate coatings are commonly used for many industrial products such as solar cells,[1] batteries[2] and so on. The properties and performance of the coatings depend on the microstructure, and it is important to understand the microstructural change during drying, which can be characterized by the particle distribution, the degree of alignment, and the coating thickness. A number of modeling and experimental studies that analyzed the microstructural change of the particulate coatings have been done. Both modeling and experimental studies emphasized the formation and the role of the close-packed region. The close-packed region is the region where the particles are closely packed with solvent filling in the interparticle void space. The capillary pressure of the meniscus in the close-packed region[3−6] and the fluid flow into or through the close-packed region[6−8] have a strong influence on the formation of the microstructure.

Routh and Zimmerman[9] and Cardinal et al.[10] predicted the particle distribution in the vertical direction of a substrate and analyzed the formation of the close-packed region during drying by solving one-dimensional conservation equation. By applying the lubrication approximation, Routh and Russel[3] predicted the particle distribution and the coating thickness in the horizontal direction and analyzed the close-packed region formed from the edge of the film during drying. Maki and Kumar[11] predicted the accumulation of particles at the liquid−air interface as well as at the edge of the droplet. Deegan et al.[12,13] showed that a ring-like deposit was produced due to the capillary flow from the center to the edge of the drop induced by the differential evaporation rates across the drop. Dimitrov and Nagayama[5] explained the role of the evaporation in the close-packed region for the convective assembly and predicted the coating thickness.

Using Cryo-SEM, Cardinal et al.[10] observed a well-ordered particle structure in the close-packed region near the coating surface under the evaporation dominant drying condition. Salamanca et al.[4] observed the movement of the boundaries of the close-packed region in the horizontal direction during drying by magnetic resonance microscopy. The movement of the boundary of the close-packed region near the meniscus was observed in the convective assembly.[5] Meng et al.,[7] Gasperino et al.,[8] and Brewer et al.[14] analyzed the crystallization mechanism in the close-packed region by microscopic observation and simulation, respectively; however, the mechanism is not fully understood yet.

Convective assembly is a representative method for the development of a well-ordered structure in the close-packed region by the fluid flow into or through the close-packed region.[7,8] The general procedure is shown in Figure 1. By placing or lifting slowly a nearly vertical substrate in the bath of a dilute suspension during drying, a thin film with an ordered particle structure develops.[6,15,16] It may well be considered as the dip coating of a dilute suspension at a very low processing speed. In analyzing the dip coating process, capillary number Ca defined as the relative strength between the viscous stress and the capillary pressure is important.

$$Ca = \frac{\mu(E + u_s)}{\gamma} \tag{1}$$

Here, μ is the solvent viscosity, γ is the solvent surface tension, E is the evaporation rate, and u_s is the drawing speed (E has the same unit as u_s). For convenience, the properties of the dilute suspension was assumed to be the same as the properties of the

Received: August 27, 2013
Revised: December 3, 2013
Published: December 4, 2013

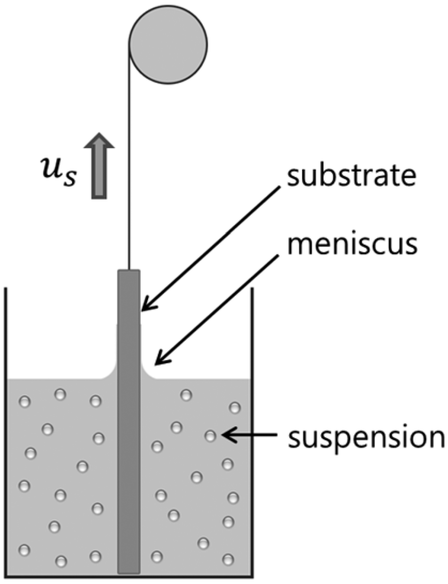

Figure 1. Schematic of the convective assembly.

solvent. Ca_0 is Ca when the drawing speed is zero. In this article, a low processing speed means that Ca is small and a high processing speed means that Ca is large.

For a large Ca, the viscous stress, which is induced by the movement of the substrate, dominates the dip coating process. This corresponds to the typical dip coating process condition, and the wet coating thickness is determined by the well-known Landau–Levich equation.[17] During drying, the particle volume fraction of the film developed by the Landau–Levich deposition increases from the initial volume fraction, ϕ_0, to the particle volume fraction of the random close packing structure, $\phi_r = 0.64$. The dry coating thickness, $h_{\mathrm{LL,dry}}$, is the wet coating thickness, $0.945 l_c Ca^{2/3}$, multiplied by $\phi_0/0.64$ as follows:

$$\frac{h_{\mathrm{LL,dry}}}{l_c} = 1.48 Ca^{2/3} \phi_0 \tag{2}$$

where $l_c = (\gamma/\rho g)^{1/2}$ is the capillary length, which represents the height of the capillary rise (ρ is the solvent density and g is the acceleration of the gravity). As Ca increases, the coating thickness increases in proportion to $Ca^{2/3}$. Ouriemi and Homsy[18] and Dixit and Homsy[19] found that the presence of surface-adsorbed hydrophobic particles results in a slightly different power law from the Landau–Levich equation. However, the effect of interfacial elasticity was neglected in this work. For the convective assembly to develop a well-ordered structure, the particle volume fraction after drying was assumed to be the particle volume fraction of the close-packed lattice structure, $\phi_m = 0.74$. In the Landau–Levich deposition, which cannot develop three-dimensional close-packed lattice structure as in the convective assembly, the particle volume fraction after drying is less than 0.74.[3,20] Here, we assumed a random close packing at $\phi_r = 0.64$.[3,9,10]

For a small Ca, the film is formed by the convective assembly. Figure 2 shows the idealized view of the close-packed region explaining the mechanism of the convective assembly. The particle packing front is the lower boundary of the close-packed region, and the drying front is the upper boundary of the close-packed region. The wet coating thickness, which is the thickness of the close-packed region, equals the coating

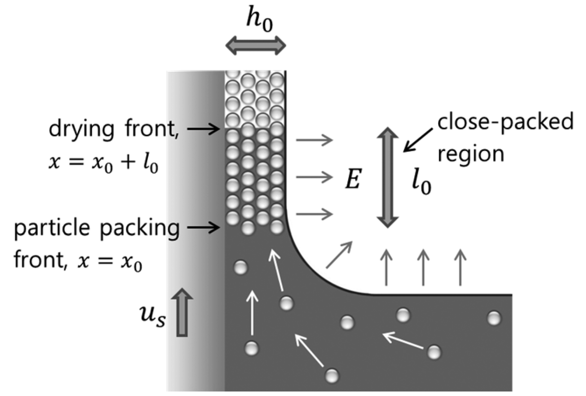

Figure 2. Idealized view of the close-packed region.

thickness of the dry film located above the drying front. l_0 and h_0 represent the length of the close-packed region and the coating thickness of the convective assembly, respectively. When Ca is small enough, the close-packed region is formed on the substrate near the meniscus at the early stage of drying and the fluid flow into or through the close-packed region due to evaporation in the close-packed region causes the convective assembly. Therefore, the coating thickness of the convective assembly is mainly affected by the evaporation in the close-packed region, not the viscous stress.

Le Berre et al.,[21] Brewer et al.,[22] and Berteloot et al.[23] measured the coating thickness of the dip coating of colloidal suspensions in a wide range of Ca from the convective assembly to the Landau–Levich deposition. They showed that the coating thickness decreases as Ca increases at the small Ca region where the film is formed by the convective assembly, while the coating thickness increases with Ca at the large Ca region where the film is formed by the Landau–Levich deposition.

To predict the coating thickness of the convective assembly, it is important to estimate the length of the close-packed region. Dimitrov and Nagayama[5] explained the role of evaporation in the close-packed region and predicted the coating thickness. Berteloot et al.[23] predicted the coating thickness using the scale of the meniscus size. However, an accurate prediction could not be made because the length of the close-packed region was either assumed to be constant or neglected. The coating thickness of the convective assembly was measured experimentally under various coating conditions,[6,15,24–26] but there have been few attempts to observe the length of the close-packed region as a function of the coating conditions.

In this study, the length of the close-packed region of the convective assembly was predicted, and the dimensionless length of the close-packed region and the dimensionless coating thickness were shown to be the functions of only three dimensionless variables: Ca, Ca_0, and ϕ_0. From the modeling results, coating process regime maps that predict the dimensionless coating thickness in terms of the dimensionless variables were created. In addition, the effects of the initial volume fraction and the evaporation rate on the length of the close-packed region were measured experimentally to validate the performance of the modeling.

2. THEORY

It is important to predict the length of the close-packed region in order to understand the convective assembly process. As the solvent flows through the close-packed region and experiences a pressure drop, the flow can be described by Darcy's law. Then the length of the close-packed region and the coating thickness can be obtained by solving the particle balance equation, the solvent balance equations and Darcy's law in the close-packed region.

To model l_0 and h_0, several assumptions were required. First, evaporation in the close-packed region was assumed to have a strong influence on the film formation. The validity of this assumption was demonstrated in the discussion on the mechanism of the convective assembly in Figure 2. Second, because h_0 is small relative to the substrate width, the edge effect was neglected. Third, the pressure drop by gravity was assumed to be negligible. In the close-packed region, the maximum capillary pressure of the spherical-cap meniscus in the pore within the close-packed particles of radius a is approximated as $10\gamma/a$ = 2.2 MPa, with a = 100 nm for alcohol.[27] This pressure is equivalent to the pressure drop caused solely by gravity with the height of a column of solvent being 290 m, which is much larger than the length scale (~mm) of the close-packed region in the experiments. So the pressure drop by gravity can be neglected in the convective assembly with the particle size being smaller than or equal to several micrometers. Fourth, the particle volume fraction was assumed to be uniform in the bath during drying because the size of the bath is large relative to that of the coated film. Fifth, h_0 was assumed to have a continuous value in the modeling, though the film has a discontinuous coating thickness because it forms layers of the close-packed particles. Also, the particles were assumed to be monodisperse hard spheres.

By equating the volumetric flow rate of the particle from the bulk solution into the particle packing front and the rate of particle accumulation, the particle balance equation at the particle packing front, $x = x_0$, can be established.

$$\phi_0 h_0 w \bar{u}_x(x_0^-) = (\phi_m - \phi_0) h_0 w (E + u_s) \tag{3}$$

The x-axis is parallel to the substrate. x_0 is the position of the particle packing front, and $x_0 + l_0$ is the position of the drying front. x_0^- is the position beneath the particle front, and x_0^+ is the position above the particle packing front. w is the width of the substrate. The particle volume fraction in the close-packed region equals ϕ_m because the particles form a close-packed lattice structure in the close-packed region. $\bar{u}_x$ is the flow rate of the fluid in the x-direction averaged over the film thickness. $\bar{u}_x$ is the flow rate of the solution below the close-packed region and becomes the flow rate of the solvent in the close-packed region where the particle movement is restrained. $\bar{u}_x(x_0^-)$ is the flow rate of the solution beneath the particle packing front. On the right-hand side of eq 3, the particles are accumulated at the particle packing front at a rate of $E + u_s$ because the substrate is drawn at a rate of u_s, and the level of the coating solution descends at the rate of E by evaporation. Then an expression for $\bar{u}_x(x_0^-)$ can be obtained as follows:

$$\bar{u}_x({x_0}^-) = \frac{(\phi_m - \phi_0)}{\phi_0}(E + u_s) \tag{4}$$

By equating the volumetric flow rate of the solvent from the bulk solution into the particle packing front and the difference between the volumetric flow rate of the solvent from the particle packing front toward the close-packed region, and the rate of reduction of the solvent due to the descent of the particle packing front, the solvent balance equation at the particle packing front, $x = x_0$, can be set up as follows:

$$\begin{aligned}(1 - \phi_0) h_0 w \bar{u}_x({x_0}^-) \\ = (1 - \phi_m) h_0 w \bar{u}_x({x_0}^+) - (\phi_m - \phi_0) h_0 w (E + u_s)\end{aligned} \tag{5}$$

where $\bar{u}_x(x_0^+)$ is the flow rate of the solvent above the particle packing front. After utilizing $\bar{u}_x(x_0^-)$ from eq 4 in eq 5, $\bar{u}_x(x_0^+)$ can be derived as follows:

$$\bar{u}_x({x_0}^+) = \frac{(\phi_m - \phi_0)}{(1 - \phi_m)\phi_0}(E + u_s) \tag{6}$$

When the volume of the solvent evaporation in the close-packed region is approximated as being equal to the volumetric flow rate of the solvent right above the particle packing front, the solvent balance equation in the closed-packed region, $x_0 < x < x_0 + l_0$, can be established.

$$l_0 w E = (1 - \phi_m) h_0 w \bar{u}_x({x_0}^+) \tag{7}$$

Then h_0 in eq 7 can be solved using $\bar{u}_x(x_0^+)$ from eq 6.

$$h_0 = \frac{\phi_0}{(\phi_m - \phi_0)\left(1 + \frac{u_s}{E}\right)} l_0 \tag{8}$$

Assuming ϕ_0 is small and substituting 0.74 for ϕ_m, the following can be obtained.

$$h_0 = 1.35 \frac{\phi_0}{\left(1 + \frac{u_s}{E}\right)} l_0 \tag{9}$$

Dimitrov and Nagayama[5] obtained the coating thickness of the convective assembly as follows:

$$k = \frac{\beta l_0 E \phi_0}{1.21 a \nu_c^{(k)} (1 - \phi_0)} \tag{10}$$

where k is the number of layers; β is the ratio between the velocity of a particle in solution and the fluid velocity, and $\nu_c^{(k)}$ is the growth rate of the k-layer array. As the particles form the close-packed lattice structure in the close-packed region, the coating thickness can be expressed as $h_0 = (2\sqrt{6/3})ka + (2 - (2\sqrt{6/3}))a$. Assuming $h_0 \gg (2 - (2\sqrt{6/3}))a$, h_0 is approximated as $(2\sqrt{6/3})ka$. After substituting $E + u_s$ for $\nu_c^{(k)}$, 1 for β and $(2\sqrt{6/3})ka$ for h_0 in eq 10 and assuming ϕ_0 is small, the same result with eq 9 can be obtained. l_0 is included in both eq 9 and eq 10. However, l_0 is not a constant and needs to be a function of the material properties and coating conditions.

The solvent flow through the close-packed region can be described by Darcy's law. l_0 can be modeled by equating the amount of pressure drop in the close-packed region calculated by Darcy's law and the maximum capillary pressure of the spherical-cap meniscus in the pore of the close-packed region.

The flow rate of the solvent in the closed-packed region, $x_0 < x < x_0 + l_0$, can be obtained from the continuity equation of the solvent. By equating the divergence of the volumetric flow rate of the solvent and the evaporation rate of the solvent, the continuity equation of the solvent in the close-packed region can be derived.

$$\frac{\partial}{\partial x}[(1 - \phi_m) h_0 w \bar{u}_x(x)] = -wE \tag{11}$$

Because the flow rate of the solvent is expressed by eq 6 above the particle packing front and is zero at the drying front, the boundary conditions on eq 11 are

$$\bar{u}_x = \frac{(\phi_m - \phi_0)}{(1-\phi_m)\phi_0}(E + u_s) \quad \text{at} \quad x = x_0^{+} \tag{12}$$

$$\bar{u}_x = 0 \quad \text{at} \quad x = x_0 + l_0 \tag{13}$$

Then $\bar{u}_x(x)$ becomes

$$\bar{u}_x(x) = \frac{(E+u_s)(\phi_m - \phi_0)}{(1-\phi_m)\phi_0}\left[1 - \frac{(x-x_0)}{l_0}\right] \tag{14}$$

The solvent flow through the close-packed region is described by Darcy's law, adapted from Routh and Russel.[3] Because in the close-packed region Reynolds number, $Re = (\rho \bar{u}_x a/\mu)$, is on the order of 10^{-6} with $E = 10^{-7}$ m/s and $a = 100$ nm, it is valid to apply Darcy's law.

$$\frac{\partial p}{\partial x} = -\frac{\mu}{k_p}(1-\phi_m)(\bar{u}_x - u_s) = -\frac{75\mu\phi_m^{\,2}}{2a^2(1-\phi_m)^2}(\bar{u}_x - u_s) \tag{15}$$

where p is the pressure and k_p is the permeability. k_p is the function of ϕ_m and a according to the Carman–Kozeny equation.[28] Because the capillary pressure has a maximum value at $x = x_0 + l_p$ where the pressure gradient becomes zero and the maximum capillary pressure of the meniscus in the close-packed region can be approximated as $10\gamma/a$,

$$p_c(x_0 + l_p) \approx \frac{10\gamma}{a} \tag{16}$$

where p_c is the capillary pressure, and l_p is the length between the particle packing front and the position where the pressure gradient is zero in the close-packed region. According to eq 15, the flow rate of the solvent equals u_s at the position where the pressure gradient is zero. By substituting $x = x_0 + l_p$ and $\bar{u}_x = u_s$ into eq 14, l_p/l_0 can be obtained.

$$\frac{l_p}{l_0} = 1 - \frac{(1-\phi_m)\phi_0}{(\phi_m - \phi_0)\left(1 + \frac{E}{u_s}\right)} \tag{17}$$

If ϕ_0 is small, the second term of the right-hand side is negligible and l_p is approximately equal to l_0. So the maximum capillary pressure appears near the drying font. By equating the amount of the pressure drop calculated by integrating eq 15 from $x = x_0$ to $x = x_0 + l_p$ after using $\bar{u}_x(x)$ from eq 14 into eq 15 and the maximum capillary pressure, the following equation is obtained:

$$-\int_{x_0}^{x_0+l_p} -\frac{75\mu\phi_m^{\,2}}{2a^2(1-\phi_m)^2}\left\{\frac{(E+u_s)(\phi_m-\phi_0)}{(1-\phi_m)\phi_0} \times \left[1 - \frac{(x-x_0)}{l_0}\right] - u_s\right\} \mathrm{d}x = \frac{10\gamma}{a} \tag{18}$$

By solving both eq 17 and eq 18, the following equation is derived:

$$l_0 = \frac{8a\gamma(1-\phi_m)^3}{15\mu E\left(1+\frac{u_s}{E}\right)\phi_m^{\,2}\left[1 - \frac{(1-\phi_m)\phi_0}{(\phi_m-\phi_0)\left(1+\frac{E}{u_s}\right)}\right]^2}\frac{\phi_0}{(\phi_m - \phi_0)} \tag{19}$$

Finally, after inserting l_0 in eq 19 into eq 8, h_0 is obtained as a function of the material properties and the coating conditions.

$$h_0 = \frac{8a\gamma(1-\phi_m)^3}{15\mu E\left(1+\frac{u_s}{E}\right)^2\phi_m^{\,2}\left[1 - \frac{(1-\phi_m)\phi_0}{(\phi_m-\phi_0)\left(1+\frac{E}{u_s}\right)}\right]^2}\frac{\phi_0^{\,2}}{(\phi_m - \phi_0)^2} \tag{20}$$

If ϕ_0 is small, the dimensionless length of the close-packed region and the dimensionless coating thickness can be expressed simply as functions of three dimensionless variables: Ca, Ca_0, and ϕ_0.

$$\frac{l_0}{a} = 0.023\frac{\gamma}{\mu(u_s + E)}\phi_0 = 0.023Ca^{-1}\phi_0 \tag{21}$$

$$\frac{h_0}{a} = 0.031\frac{\gamma E}{\mu(u_s + E)^2}\phi_0^{\,2} = 0.031Ca_0Ca^{-2}\phi_0^{\,2} \tag{22}$$

When $u_s = 0$, eq 22 yields

$$\frac{h_0}{a} = 0.031Ca_0^{\,-1}\phi_0^{\,2} \tag{23}$$

3. EXPERIMENTAL METHODS

A model system of monodisperse silica particles in alcohol was used to compare the modeling results to the experiments. While keeping the substrate fixed, l_0 was measured under various coating conditions with different ϕ_0 and E.

Monodisperse silica particles of 200 nm ± 7% in diameter were synthesized using the Stober method.[29] Figure 3 shows the SEM image of the particles. The particles were suspended in alcohol. Eighteen milliliters of coating solution were added in a 30 mm × 30 mm × 30 mm glass cell and dried in a sealed box at 22 °C. Sealed boxes of different sizes, 8 L, 40 L, and 150 L, were used to control the evaporation rate. Because the experiments were performed only for $u_s = 0$, the inner wall of the glass cell could be substituted for the substrate. While the particles were being coated on the inner wall of the glass cell, l_0 was measured by taking the images of the wall using a CCD

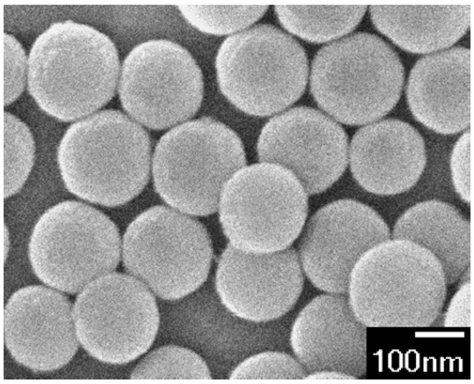

Figure 3. SEM image of the silica particles.

camera. Because the solution concentration in the glass cell increases as drying proceeds, l_0 was measured when the free surface descended to an equal length of 5 mm. E was determined by measuring the level of the free surface from the images.

Figure 4 shows the image of the inner wall of the glass cell with a black background. The close-packed region looks substantially transparent because it is a thin film with solvent filled in the interparticle void space. A dried film (white color) is formed above the close-packed region. Below the close-packed region, the coating solution in the glass cell looks white. So the black area between the two white areas is the close-packed region. The upper boundary of the black area is the drying front, and the lower boundary is the particle packing front.

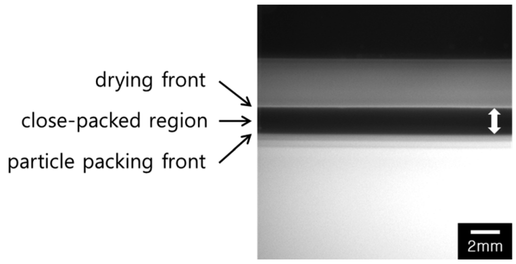

Figure 4. Image of the close-packed region.

4. RESULTS AND DISCUSSION

Modeling Results. The dimensionless length of the close-packed region and the dimensionless coating thickness are the functions of the three dimensionless variables: Ca, Ca_0, and ϕ_0. Comparing eq 22 and eq 23 with eq 2, the dimensionless coating thicknesses of the convective assembly and the Landau–Levich deposition have the same form, but are different only in the values of the exponents of the dimensionless variables. In the Landau–Levich equation, the dimensionless coating thickness is proportional to $Ca^{2/3}$ and ϕ_0. In the convective assembly, the dimensionless coating thickness is proportional to $Ca_0^{\,1}Ca^{-2}$ for the moving substrate, eq 22, or $Ca_0^{\,-1}$ for the static substrate, eq 23, and $\phi_0^{\,2}$. The Landau–Levich equation is applied when the close-packed region cannot be developed and the viscous stress mainly affects the dip coating process because Ca is large. The coating thickness of the Landau–Levich deposition increases as Ca increases. On the other hand, the convective assembly is applied when the close-packed region is formed on the substrate near the meniscus at the early stage of drying because Ca is small. As Ca increases, the coating thickness of the convective assembly decreases because l_0 is decreased due to the increase in the pressure drop or the decrease in the maximum capillary pressure in the close-packed region.

Comparing eq 22 with eq 9 or Dimitrov and Nagayama's result (eq 10), l_0, which is a constant in eq 9 and eq 10, is replaced by l_0 from eq 21. Additionally, h_0 now depends not only on the coating conditions, E, u_s, and ϕ_0, but also on the material properties of the suspension, a, γ, and μ.

In eq 22, h_0 is shown as a function of the material properties (a, γ, μ) and the coating conditions (E, u_s, ϕ_0). When $u_s < E$ or $u_s = 0$, l_0 decreases with the increase in the pressure drop in the close-packed region as μ, E, and u_s increase, and thus, h_0 decreases. When $u_s > E$, h_0 decreases as μ and u_s increase, but h_0 increases with E according to eq 22. This is because when $u_s > E$, the pressure drop is predominantly determined by u_s rather than E, and an increase in E increases the amount of the evaporation and enhances the particle packing at the particle packing front. As γ increases, the maximum capillary pressure increases, and l_0 as well as h_0 increases. As a increases, l_0 increases because the pressure drop is reduced by $1/a^2$ while the maximum capillary pressure is reduced by $1/a$. Therefore, h_0 increases. As ϕ_0 increases, both l_0 and h_0 increase because more particles accumulate at the particle packing front.

Coating Process Regime Maps. Using the modeling result for the static substrate, eq 23, a coating process regime map that predicts the coating thickness in terms of the dimensionless variables, ϕ_0 and Ca_0, was created, as shown in Figure 5. The coating thickness of the film formed by the convective assembly is discontinuous because the film has a structure consisting of the stacking of layers of hexagonally close-packed particles. Thus, the coating thickness was expressed as the number of layers, n, instead of the dimensionless coating thickness in the coating process regime map. The film has a monolayer when $(h_0/a) = 2$, a bilayer when $(h_0/a) = 3.633$, and n layers when $(h_0/a) = 2 + (2\sqrt{6}/3)(n - 1)$. When n is an integer, the film with uniform coating thickness of n layers is formed because the growth rate of the film balances the difference in the velocities of substrate withdrawal and the descent of the surface of coating solution.[5] However, when n is not an integer, a difference between the growth rate of the film and the velocity of substrate withdrawal relative to the descent of the surface exists. The meniscus between the surface of coating solution and the particle packing front changes with time, so uneven film[22] with average coating thickness of n layers or stripe pattern[30,31] appears. However, the mechanism of the film formation is not fully understood yet. The different shapes of the lines represent the coating conditions for the monolayer, bilayer, 10 layers, and 100 layers, respectively. The slopes of the lines are 1/2 because the dimensionless coating thickness is proportional to $\phi_0^{\,2}$ and $Ca_0^{\,-1}$. As ϕ_0 increases or Ca_0 decreases, h_0 increases.

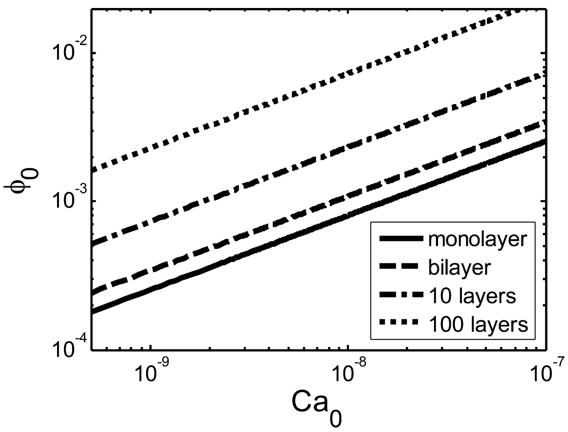

Figure 5. Coating process regime map for the static substrate.

In eq 22, the dimensionless coating thickness is expressed as the function of the three dimensionless variables, Ca, Ca_0, and ϕ_0. Because Ca_0 and Ca are not independent, a coating process regime map for the moving substrate was created in terms of Ca_0 and Ca while changing ϕ_0 shown in Figure 6. The thick lines represent the coating conditions for $\phi_0 = 0.01$ and the thin lines for $\phi_0 = 0.001$. The different shapes of the lines represent

dx.doi.org/10.1021/la4033139 | Langmuir 2013, 29, 15762−15769

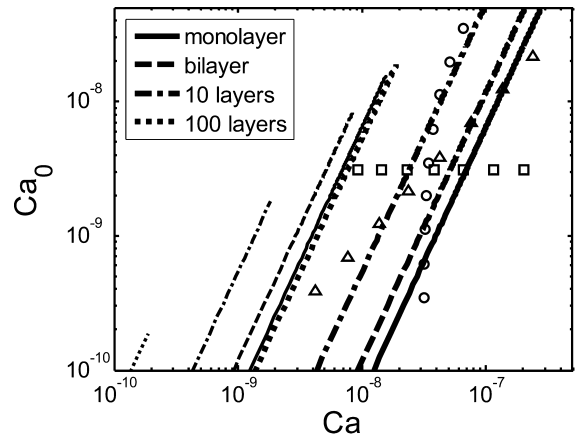

Figure 6. Coating process regime map for the moving substrate: ϕ_0 = 0.01 (thick lines), ϕ_0 = 0.001 (thin lines), the effect of E on h_0 (○), the effect of γ or μ on h_0 (△), the effect of u_s on h_0 (□).

the coating conditions for the monolayer, bilayer, 10 layers, and 100 layers. In the upper left corner of the map where Ca is smaller than Ca_0, the map was not drawn because $u_s < 0$. The slopes of the lines are 2 because the dimensionless coating thickness is proportional to Ca_0 and Ca^{-2}. If ϕ_0 is reduced, Ca needs to be reduced in order to form a film of the same coating thickness at a constant Ca_0. Therefore, the regime for ϕ_0 = 0.001 lies on the left-hand side of the regime for ϕ_0 = 0.01, and h_0 increases as ϕ_0 increases for the same Ca_0 and Ca. Circle markers show the effect of E on h_0. The value of E increases as Ca_0 and Ca increase. As E increases, h_0 increases when $u_s > E$, but h_0 decreases when $u_s < E$. Triangle markers show the effect of γ or μ on h_0. The value of γ decreases or the value of μ increases as Ca_0 and Ca increase. As γ decreases or μ increases, h_0 decreases. Square markers show the effect of u_s on h_0. The value of u_s increases as Ca increases, and h_0 decreases as u_s increases.

Using eq 2 for the Landau−Levich deposition and eq 22 for the convective assembly, a coating process regime map in terms of the dimensionless variables, ϕ_0 and Ca, with a constant Ca_0 was created, as shown in Figure 7. The thick lines represent the coating conditions of the films being formed by the convective assembly and the thin lines by the Landau−Levich deposition. The different shapes of the lines represent the coating conditions for the monolayer, bilayer, 10 layers and 100 layers. Ca_0 was fixed at 1×10^{-9}. h_0 in eq 22 is nondimensionalized by a, and the dimensionless coating thickness is independent of a. However, $h_{LL,dry}$ in eq 2 is nondimensionalized by l_c and if it is nondimensionalized by a in order to fit in the same graph with eq 22, the dimensionless coating thickness will be inversely proportional to a. Therefore, a was fixed at 100 nm only for eq 2. The coating thickness of the Landau−Levich deposition for an arbitrary a can be obtained by multiplying the coating thickness predicted by the coating process regime map by 100 nm/a. If a = 200 nm and the coating condition is located in the convective assembly regime (upper left part of the map), we can use the coating thickness predicted by the coating process regime map. However, if the coating condition is located in the Landau−Levich deposition regime (upper right part of the map), we need to multiply the coating thickness predicted by the coating process regime map by (100 nm/200 nm) = 0.5. The slopes of the thick lines in the convective assembly regime are 1 because the coating thickness is proportional to ϕ_0^2 and Ca^{-2}, and the slopes of the thin lines in the Landau−Levich deposition regime are −2/3 because the coating thickness is proportional to ϕ_0 and $Ca^{2/3}$. At a small Ca, the film is formed by the convective assembly with the close-packed lattice structure, and the coating thickness decreases with Ca. If Ca continues to increase, the coating condition falls into the Landau−Levich deposition regime. At the onset of the Landau−Levich deposition regime, where a transition between the convective assembly and the Landau−Levich deposition is realized, the close-packed monolayer can be developed.[22] However, except at this transition, the film does not form a well-ordered structure as in the convective assembly, and the coating thickness increases as Ca increases. As ϕ_0 increases, the coating thickness increases both in the convective assembly regime and in the Landau−Levich deposition regime. Using this coating process regime map, one can predict the coating mechanism (convective assembly or Landau−Levich deposition), the degree of particle alignment (close-packed lattice structure or less ordered structure) and the coating thickness according to ϕ_0 and Ca under certain dip coating process conditions.

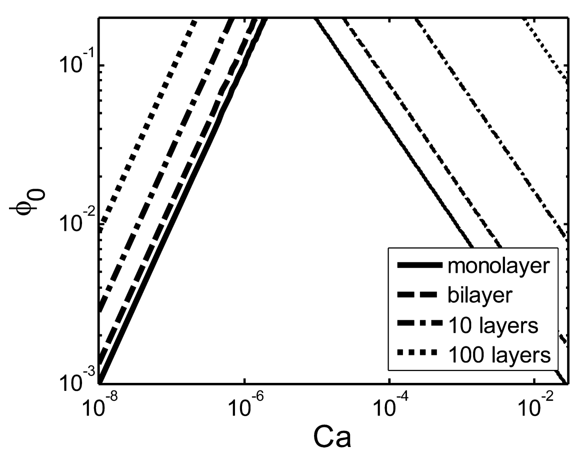

Figure 7. Coating process map for the moving substrate when Ca_0 is fixed: Convective assembly (thick lines), Landau−Levich deposition (thin lines).

■ EXPERIMENTAL SECTION

When u_s = 0, l_0 was measured under the various coating conditions with different ϕ_0 and E using a model system of monodisperse silica particles in alcohol. Table 1 shows the experimentally explored coating conditions and the average values of the measured l_0. In the first four coating conditions l_0 increased with ϕ_0, and in the next, l_0 decreased with E.

Table 1. Experimentally Explored Coating Conditions

ϕ_0	E [m/s]	Ca_0	l_0 [m]
0.001	9.7×10^{-8}	5.2×10^{-9}	0.8×10^{-3}
0.0025	9.7×10^{-8}	5.2×10^{-9}	1.4×10^{-3}
0.005	9.7×10^{-8}	5.2×10^{-9}	1.8×10^{-3}
0.01	9.7×10^{-8}	5.2×10^{-9}	2.7×10^{-3}
0.0025	3.6×10^{-8}	1.9×10^{-9}	2.9×10^{-3}
0.0025	6.1×10^{-8}	3.3×10^{-9}	2.0×10^{-3}
0.0025	9.7×10^{-8}	5.2×10^{-9}	1.4×10^{-3}

Figure 8 shows the experimental results of the dependence of l_0 on ϕ_0. The error bars represent the standard deviations of l_0. The slope of the graph is 0.52 and l_0 was found to be proportional to $\phi_0^{0.52}$. According to eq 21, l_0 is proportional to ϕ_0 when u_s = 0. Both the

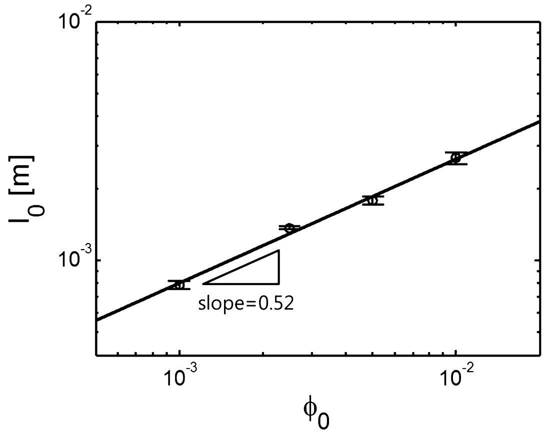

Figure 8. Dependence of the length of the close-packed region on the initial volume fraction.

experiments and modeling showed the trend of l_0 increasing with the increase in ϕ_0. However, in the experiments, the exponent of ϕ_0 was measured to be smaller than the modeling. Figure 9 shows the

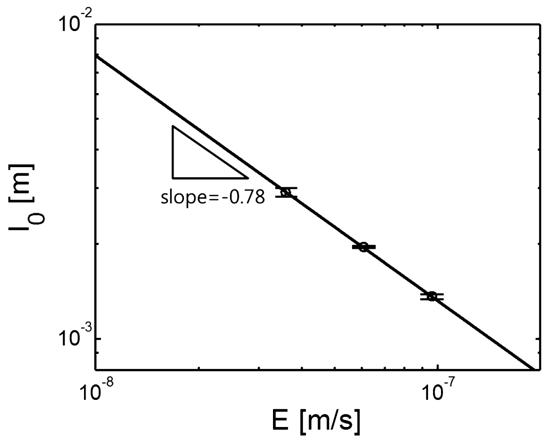

Figure 9. Dependence of the length of the close-packed region on the evaporation rate.

experimental results on the effects of E. The slope of the graph is −0.78 and l_0 was proportional to $E^{-0.78}$. In eq 21 of the modeling, l_0 is proportional to E^{-1} when $u_s = 0$. Both the experiments and modeling showed the trend of l_0 decreasing with the increase in E. However, in the experiments, the absolute value of the exponent of E was measured to be smaller than the model prediction. In the experiments on the effects of ϕ_0 and E, the absolute values of the exponents of both variables were measured to be smaller than the modeling. In addition, the difference between the experiments and the modeling was larger for the dependence on ϕ_0 than that on E.

One of the possible causes for the differences is that l_0 could be measured to be larger than the actual length in the experiments. In Figure 2, the particle packing front is located slightly above the surface of the coating solution due to the meniscus being formed in the position where the surface of the coating solution and the substrate meet. l_0 was determined experimentally by measuring the length of the transparent area between the two white areas shown in Figure 4 without observing the particles in the close-packed region directly. Therefore, l_0 could be measured larger than the actual length by including part of the meniscus. If l_0 was assumed to be measured 0.2×10^{-3} m larger, l_0 could be recalculated to be proportional to ${\phi_0}^{0.61}$ and $E^{-0.87}$, which becomes more consistent with the modeling results. Furthermore, if we assume that l_0 was measured 0.43×10^{-3} m larger, the experiments and the modeling would coincide on the effect of E on l_0. It is possible that a greater part of the meniscus was included in determining l_0 for the coating solution with a low ϕ_0 because the coating solution with a low ϕ_0 is more transparent than a high ϕ_0. Therefore, the effect of ϕ_0 on l_0 could be measured to be much smaller.

If the pressure drop is proportional to the nth power of the flow rate (n less than 1), the modeling can predict the experimental results more closely. Darcy's law that was used to determine l_0 in the modeling describes the pressure drop when the Newtonian fluid goes through the packed bed composed of the monodisperse hard spheres. Because the model system used in the experiments was not a perfect monodisperse hard sphere, by assuming that the pressure drop in the close-packed region was proportional to the nth power of the flow rate, l_0 could be rederived. When $u_s = 0$, Darcy's law was modified according to the assumptions above.

$$\frac{\partial p}{\partial x} = -\frac{\mu}{k_{p,n}(a)}(1 - \phi_m)^n \bar{u}_x^{\,n} \tag{24}$$

where $k_{p,n}$ is the permeability of the modified Darcy's law. Because k_p from eq 15 is the function of a, $k_{p,n}$ was also assumed to be the function of a. The dependence of the permeability on ϕ_m was not considered because ϕ_m is a constant. By substituting $u_s = 0$ into eq 17, $l_p = l_0$ was recovered. By equating the amount of the pressure drop calculated by integrating eq 24 from $x = x_0$ to $x = x_0 + l_0$ after utilizing $\bar{u}_x(x)$ from eq 14 and the maximum capillary pressure, the following equation was obtained:

$$-\int_{x_0}^{x_0+l_0} -\frac{\mu(1-\phi_m)^n}{k_{p,n}(a)}\left\{\frac{E(\phi_m-\phi_0)}{(1-\phi_m)\phi_0}\left[1-\frac{(x-x_0)}{l_0}\right]\right\}^n \mathrm{d}x = \frac{10\gamma}{a} \tag{25}$$

After solving l_0 in eq 25 and assuming ϕ_0 is small, l_0 was derived as

$$l_0 = \frac{\gamma f_n(a)}{\mu}\frac{{\phi_0}^n}{E^n} \tag{26}$$

where $f_n(a) = (10(n + 1)/a{\phi_m}^n)k_{p,n}(a)$. Inserting l_0 from eq 26 into eq 9, h_0 was obtained.

$$h_0 = \frac{1.35\gamma f_n(a)}{\mu}\frac{{\phi_0}^{n+1}}{E^n} \tag{27}$$

In eq 26, l_0 is proportional to ${\phi_0}^n$ and E^{-n}. If $n = 0.52$, the modeling results can explain the experimental results of the effect of ϕ_0. Also, if $n = 0.78$, the modeling can describe well the experimental results of the effect of E.

5. CONCLUSIONS

In this work, the length of the close-packed region and the coating thickness were predicted by combining Darcy's law with the particle and solvent balance equations in the close-packed region. The dimensionless length of the close-packed region and the dimensionless coating thickness were found to be the functions of only three dimensionless variables: Ca, Ca_0, and ϕ_0. From the modeling results, coating process regime maps that predict the dimensionless coating thickness in terms of the dimensionless variables were created. By using the coating process regime map which combines the Landau−Levich deposition regime altogether, one can predict the mechanism (convective assembly or Landau−Levich deposition), the degree of particle alignment and the coating thickness in terms of Ca and ϕ_0 under an arbitrary dip coating process. In addition, the effects of the initial volume fraction and the evaporation rate on the length of the close-packed region were observed experimentally to validate the model prediction. Both the experiments and modeling showed the same tendency that the length of the close-packed region increased with an increase in the initial volume fraction or a decrease in the evaporation rate. However, the measured absolute values of the exponents were found to be smaller than the model prediction. The discrepancy may be attributed to the inclusion of the meniscus during the measurement of the length of the close-packed region. When the pressure drop was assumed to be proportional to the *n*th power of the flow rate, the modeling could fit the experimental results.

■ AUTHOR INFORMATION

Corresponding Author

*E-mail: ahnnet@snu.ac.kr.

Notes

The authors declare no competing financial interest.

■ ACKNOWLEDGMENTS

This work was supported by a National Research Foundation of Korea (NRF) grant (No. 20100026139) funded by the Korean government (MEST).

■ REFERENCES

(1) O'regan, B.; Grfitzeli, M. A low-cost, high-efficiency solar cell based on dye-sensitized colloidal TiO_2 Films. *Nature* **1991**, *353*, 737−740.

(2) Yun, M.-S.; Jeong, K.-Y.; Lee, E.-W.; Jin, B.-S.; Moon, S.-I.; Doh, C.-H. A study on carbon coating to silicon and electrochemical characteristics of Si-C/Li cells. *Korean J. Chem. Eng.* **2006**, *23*, 230−236.

(3) Routh, A. F.; Russel, W. B. Horizontal drying fronts during solvent evaporation from latex films. *AIChE J.* **1998**, *44*, 2088−2098.

(4) Salamanca, J.; Ciampi, E.; Faux, D.; Glover, P.; McDonald, P.; Routh, A.; Peters, A.; Satguru, R.; Keddie, J. Lateral drying in thick films of waterborne colloidal particles. *Langmuir* **2001**, *17*, 3202−3207.

(5) Dimitrov, A. S.; Nagayama, K. Continuous convective assembling of fine particles into two-dimensional arrays on solid surfaces. *Langmuir* **1996**, *12*, 1303−1311.

(6) Fustin, C.-A.; Glasser, G.; Spiess, H. W.; Jonas, U. Parameters influencing the templated growth of colloidal crystals on chemically patterned surfaces. *Langmuir* **2004**, *20*, 9114−9123.

(7) Meng, L.; Wei, H.; Nagel, A.; Wiley, B. J.; Scriven, L. E.; Norris, D. J. The role of thickness transitions in convective assembly. *Nano Lett.* **2006**, *6*, 2249−53.

(8) Gasperino, D.; Meng, L.; Norris, D. J.; Derby, J. J. The role of fluid flow and convective steering during the assembly of colloidal crystals. *J. Cryst. Growth* **2008**, *310*, 131−139.

(9) Routh, A. F.; Zimmerman, W. B. Distribution of particles during solvent evaporation from films. *Chem. Eng. Sci.* **2004**, *59*, 2961−2968.

(10) Cardinal, C. M.; Jung, Y. D.; Ahn, K. H.; Francis, L. F. Drying regime maps for particulate coatings. *AIChE J.* **2010**, *56*, 2769−2780.

(11) Maki, K. L.; Kumar, S. Fast evaporation of spreading droplets of colloidal suspensions. *Langmuir* **2011**, *27*, 11347−11363.

(12) Deegan, R. D.; Bakajin, O.; Dupont, T. F.; Huber, G.; Nagel, S. R.; Witten, T. A. Capillary flow as the cause of ring stains from dried liquid drops. *Nature* **1997**, *389*, 827−829.

(13) Deegan, R. D.; Bakajin, O.; Dupont, T. F.; Huber, G.; Nagel, S. R.; Witten, T. A. Contact line deposits in an evaporating drop. *Phys. Rev. E* **2000**, *62*, 756−765.

(14) Brewer, D. D.; Allen, J.; Miller, M. R.; de Santos, J. M.; Kumar, S.; Norris, D. J.; Tsapatsis, M.; Scriven, L. Mechanistic principles of colloidal crystal growth by evaporation-induced convective steering. *Langmuir* **2008**, *24*, 13683−13693.

(15) Jiang, P.; Bertone, J.; Hwang, K.; Colvin, V. Single-crystal colloidal multilayers of controlled thickness. *Chem. Mater.* **1999**, *11*, 2132−2140.

(16) Marlow, F.; Sharifi, P.; Brinkmann, R.; Mendive, C. Opals: Status and prospects. *Angew. Chem., Int. Ed.* **2009**, *48*, 6212−6233.

(17) Landau, L.; Levich, B. Dragging of a liquid by a moving plate. *Acta Physicochim. U.R.S.S.* **1942**, *17*, 42−54.

(18) Ouriemi, M.; Homsy, G. M. Experimental study of the effect of surface-absorbed hydrophobic particles on the Landau−Levich law. *Phys. Fluids* **2013**, *25*, 082111.

(19) Dixit, H. N.; Homsy, G. The elastic Landau−Levich problem. *J. Fluid Mech.* **2013**, *732*, 5−28.

(20) Russel, W. B. On the dynamics of the disorder−order transition. *Phase Transitions* **1990**, *21*, 127−137.

(21) Le Berre, M.; Chen, Y.; Baigl, D. From convective assembly to Landau−Levich deposition of multilayered phospholipid films of controlled thickness. *Langmuir* **2009**, *25*, 2554−2557.

(22) Brewer, D. D.; Shibuta, T.; Francis, L.; Kumar, S.; Tsapatsis, M. Coating process regimes in particulate film production by forced-convection-assisted drag-out. *Langmuir* **2011**, *27*, 11660−11670.

(23) Berteloot, G.; Daerr, A.; Lequeux, F.; Limat, L. Dip coating with colloids and evaporation. *Chem. Eng. Process.* **2012**, *68*, 69−73.

(24) Vlasov, Y. A.; Bo, X.-Z.; Sturm, J. C.; Norris, D. J. On-chip natural assembly of silicon photonic bandgap crystals. *Nature* **2001**, *414*, 289−293.

(25) Zhou, Z.; Zhao, X. Flow-controlled vertical deposition method for the fabrication of photonic crystals. *Langmuir* **2004**, *20*, 1524−1526.

(26) Im, S. H.; Kim, M. H.; Park, O. O. Thickness control of colloidal crystals with a substrate dipped at a tilted angle into a colloidal suspension. *Chem. Mater.* **2003**, *15*, 1797−1802.

(27) Brown, G. L. Formation of films from polymer dispersions. *J. Polym. Sci.* **1956**, *22*, 423−434.

(28) Carman, P. Fluid flow through granular beds. *Trans.-Inst. Chem. Eng.* **1937**, *15*, 150−166.

(29) Stöber, W.; Fink, A.; Bohn, E. Controlled growth of monodisperse silica spheres in the micron size range. *J. Colloid Interface Sci.* **1968**, *26*, 62−69.

(30) Watanabe, S.; Inukai, K.; Mizuta, S.; Miyahara, M. T. Mechanism for Stripe Pattern Formation on Hydrophilic Surfaces by Using Convective Self-Assembly. *Langmuir* **2009**, *25*, 7287−7295.

(31) Lee, J. A.; Reibel, K.; Snyder, M. A.; Scriven, L.; Tsapatsis, M. Geometric model describing the banded morphology of particle films formed by convective assembly. *ChemPhysChem* **2009**, *10*, 2116−2122.